WOOD RESEARCH
61 (6): 2016
951-958

FRACTURE TOUGHNESSES OF INTERLAMINAR FRACTURE OF GLUED-LAMINATED TIMBER

Bo-Han Xu, Yan-Hua Zhao, Jing-Hua Guo, Ya-Xun Wang
Dalian University of Technology, State Key Laboratory
of Coastal and Offshore Engineering
Dalian, China

(Received March 2016)

ABSTRACT

Critical strain energy release rate G_C and stress intensity factor K_C are both defined as fracture toughness, and they can be converted to one another through an equivalent elastic modulus for wood fracture. Whereas the equivalent elastic modulus for interlaminar fracture toughness of glued-laminated timber (glulam) is kept unknown. This paper briefly presented Modes I and II interlaminar fracture toughnesses of glulam, which were obtained from double cantilever beam (DCB) and three-point bending end-notched flexure (3ENF) tests using finite element method (FEM). On the basis of Hankinson-type formula and equivalent elastic modulus of wood fracture, this study developed two empirical expressions to calculate the equivalent elastic moduli for Modes I and II interlaminar fracture of glulam.

KEYWORDS: Glulam; interlaminar fracture; fracture toughness; equivalent elastic modulus.

INTRODUCTION

Glulam is now becoming a more widely used material in modern timber buildings due to its extraordinary merits, thus its mechanical properties are now the focus of researches. The study of glulam in terms of fracture mechanics has already commenced and gained some promising results. As known, two types of fractures could occur in glulam members: intralaminar fracture and interlaminar fracture. Intralaminar fracture is in essence the fracture in wood per se, while interlaminar fracture occurs at the interface of two adjacent laminae. Since the occurrence of flaws, such as small cracks, voids, or some combinations, is not completely avoidable in the manufacture processing of glulam, it is necessary to investigate its interlaminar fracture.

Fracture toughness is an indication of the amount of stress required to propagate a preexisting flaw. Accordingly, the critical stress intensity factor K_C can be used to denote the fracture toughness for most materials. Fracture toughness can also be described by critical strain energy release rate G_C, which is the measurement of energy dissipated during fracture per unit of a newly created fracture surface area.

For plane stress problems that involve a crack moving in a straight path, the stress intensity factor K is related to the energy release rate G within the linear elastic fracture mechanics range by:

$$G = \frac{K^2}{E^*} \tag{1}$$

where: E^*- the equivalent elastic modulus.
For isotropic materials $E^* = E$, E is the Young's modulus; for wood-like orthotropic materials,
E^* - was given by Sih et al. (1965) as follows:

$$\frac{1}{E_{\mathrm{I}}^*} = \frac{1}{E_x}\sqrt{\frac{E_x}{2E_y}}\sqrt{\sqrt{\frac{E_x}{E_y}} + \frac{E_x}{2G_{xy}} - \mu_{yx}\frac{E_x}{E_y}} \tag{2}$$

$$\frac{1}{E_{\mathrm{II}}^*} = \frac{1}{\sqrt{2}E_x}\sqrt{\sqrt{\frac{E_x}{E_y}} + \frac{E_x}{2G_{xy}} - \mu_{yx}\frac{E_x}{E_y}} \tag{3}$$

where: E_x - Young's modulus along the x-axis, which coincides with the fiber direction;
E_y - Young's modulus along the height of specimen;
G_{xy} - Shear modulus;
μ_{yx} - Poisson's ratio.

The equivalent elastic modulus has been validated and used to convert G_C to K_C for wood fracture (Xu et al. 1996; Susanti et al. 2011).

However, the equivalent elastic modulus for interlaminar fracture of glulam is not available in literature, and this is the objective of the present paper. To this end, DCB and 3ENF interlaminar fracture tests of glulam (Xu et al. 2016) were first briefly reviewed. The experimental results were afterwards used to calculate Modes I and II critical strain energy release rates G_{IC} and G_{IIC}, and critical stress intensity factors K_{IC} and K_{IIC}, through FEM. On the basis of Hankinson-type formula and equivalent elastic modulus of wood fracture, empirical expressions were derived to calculate equivalent elastic moduli for Modes I and II interlaminar fracture of glulam.

MATERIAL AND METHODS

In order to be easier for readers to follow this study, the DCB and 3ENF interlaminar fracture tests of glulam were briefly reviewed, and the detail can be found in the literature (Xu et al. 2016). The glulam used in the tests was made of two Mongolian Scotch pine (*Pinus sylvestris* var. *mongolica* Litv.) laminae with a thickness of 30 mm bonded by the water-based vinyl polyurethane adhesives. Tabs. 1 and 2 show main material properties of wood lamina, in which E is Young's modulus, G is shear modulus and μ is Poisson's ratio. The subscripts represent longitudinal (L), radial (R), and tangential (T) directions.

Tab. 1: Measured wood lamina properties (MPa).

E_L	E_R	E_T	G_{LR}	G_{LT}	G_{RT}
11464	1187	697	758	673	54

Tab. 2: Poisson's ratio of wood lamina.

μ_{LR}	μ_{LT}	μ_{RL}	μ_{RT}	μ_{TL}	μ_{TR}
0.370	0.638	0.037	0.765	0.030	0.387

Total of 76 DCB specimens and 90 3ENF specimens were used to perform Modes I and II interlaminar fractures, and Figs. 1 and 2 show the test configurations.

A precrack along the grain was located at the interface of the two wood laminae. According to the standardized methods (JSA 1996; ASTM 2002), the critical load for crack propagation P_C is defined as the load at the onset of nonlinearity from the load vs. loading-line displacement curves.

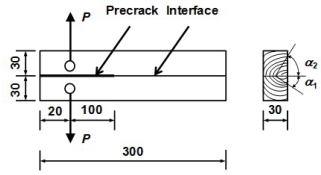

Fig. 1: Experimental geometries of DCB tests (mm).

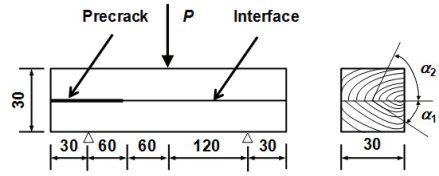

Fig. 2: Experimental geometries of 3ENF tests (mm).

To identify growth ring orientations of two adjacent laminae, digital photographs for cross section of all specimens were taken before testing, and then were imported into AutoCAD2013 for analysis. The angles between the interface line and tangent line to lamina growth ring close to the center point of specimen cross section were measured to represent the growth ring orientations. The lamina with smaller angle α_1 is defined as the lower lamina, the lamina with larger angle α_2 is defined as the upper lamina, and the angel $\alpha_{2\text{-}1}$ is defined as the difference between α_2 and α_1.

The critical load P_C slightly increases with the increase of angle $\alpha_{2\text{-}1}$ in DCB tests, and the variation of critical loads P_C is not obvious with the increase of angle $\alpha_{2\text{-}1}$ in 3ENF tests. Considering that α_1 and α_2 of tested specimens are almost in the range from 0° to 50°, a series of numerical simulations were performed corresponding to α_1 and α_2 equal to 0, 10, 20, 30, 40, and 50°, respectively.

Tab. 3: Applied load in FEM for DCB tests (N).

α_1 \ α_2	0°	10°	20°	30°	40°	50°
0°	467	448	510	430	572	539
10°		467	448	510	430	572
20°			467	448	510	430
30°				467	448	510
40°					467	448
50°						467

Tab. 4: Applied load in FEM for 3ENF tests (N).

α_1 \ α_2	0°	10°	20°	30°	40°	50°
0°	3411	3400	3553	3676	3176	a—
10°		3411	3400	3553	3676	3176
20°			3411	3400	3553	3676
30°				3411	3400	3553
40°					3411	3400
50°						3411

[a] Due to the lack of P_C corresponding to $\alpha_{2\text{-}1}$ equal to 50° from tests.

The average of the critical load P_C corresponding to $\alpha_{2\text{-}1}$ from tests was adopted as the applied load in the numerical simulation, which was summarized in Tabs. 3 and 4.

RESULTS AND DISCUSSION

Stress intensity factors

The stress intensity factors (SIFs) were calculated using the stress extrapolation method. The three-dimensional FEM was conducted using ABAQUS 6.12 (Dassault Systémes Simulia Corp. 2012). The meshing based on 8-node quadratic bricks (C3D8) and deformation of models with α_1 and α_2 equal to 30° are shown in Figs. 3 and 4.

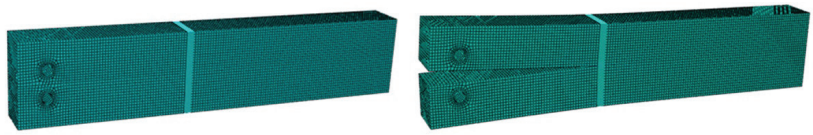

Fig. 3: Meshing and deformation of model of DCB specimen.

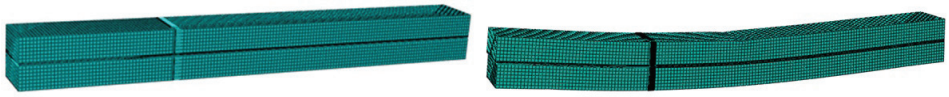

Fig. 4: Meshing and deformation of model of 3ENF specimen.

The mesh was progressively graded in order to reduce computational cost and was refined near the crack tip to best capture the crack tip stress singularity. The models were assumed to be with the zero thickness of the adhesive layer. The crack was introduced into the model using the seam option provided in ABAQUS. Moreover, in the simulation of 3ENF tests, contact algorithms incorporated in the program were used to prevent the crack surfaces from intersecting, and the frictional force induced between the crack surfaces was ignored.

SIFs may be calculated using near-tip stress fields as follows:

$$\begin{cases} K_{\mathrm{I}} = \lim\limits_{r\to 0} \sqrt{2\pi r}\,\sigma_{\mathrm{yy}}\big|_{\theta=0^\circ} \\ K_{\mathrm{II}} = \lim\limits_{r\to 0} \sqrt{2\pi r}\,\tau_{\mathrm{xy}}\big|_{\theta=0^\circ} \end{cases} \tag{4}$$

Its first step is computing $\sqrt{2\pi r}\sigma_{yy}$ on series of nodes along the ligament distance from the crack tip direction (θ = 0º). Then, a linear regression analysis of these estimates versus ligament distance is performed and extrapolation to zero gives the SIF value.

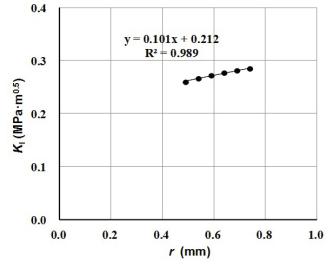

Fig. 5: Stress extrapolation in the FEM calculations of DCB test with α_1 and α_2 equal to 30°.

Fig. 5 shows the stress extrapolation in the FEM calculations of DCB test with α_1 and α_2 equal to 30°. The fracture toughnesses K_{IC} and K_{IIC} calculated using the procedure above are summarized in Tabs. 5 and 6.

Tab. 5: K_{IC} calculated by FEM (MPa$\sqrt{m}$).

α_1 \ α_2	0°	10°	20°	30°	40°	50°
0°	0.214	0.206	0.237	0.200	0.249	0.226
10°		0.214	0.206	0.236	0.198	0.246
20°			0.214	0.205	0.233	0.223
30°				0.212	0.201	0.228
40°					0.200	0.192
50°						0.185

Tab. 6: K_{IIC} calculated by FEM (MPa$\sqrt{m}$).

α_1 \ α_2	0°	10°	20°	30°	40°	50°
0°	0.651	0.648	0.677	0.700	0.603	a—
10°		0.642	0.640	0.693	0.689	0.593
20°			0.618	0.615	0.640	0.659
30°				0.575	0.571	0.593
40°					0.514	0.509
50°						0.435

[a] Due to the lack of P_C corresponding to $\alpha_{2\text{-}1}$ equal to 50° obtained from tests.

Strain energy release rate

Modes I and II interlaminar fracture toughnesses of glulam, G_{Ic} and G_{IIc}, have been calculated using FEM by Xu et al. (2016) and the results are shown in Tabs. 7 and 8.

Equivalent elastic moduli

As G_{Ic} and G_{IIc}, as well as K_{Ic} and K_{IIc} are known, the Modes I and II interlaminar fracture equivalent elastic moduli E^*_I and E^*_{II} can be obtained by using Eq. (1), respectively. The

interlaminar fracture equivalent elastic modulus should be related to equivalent elastic moduli of adjacent laminae.

Tab. 7: GIC calculated by FEM (J.m^{-2}).

α_1 \ α_2	0°	10°	20°	30°	40°	50°
0°	84	79	107	79	143	127
10°		88	84	114	83	146
20°			96	92	122	87
30°				105	99	128
40°					110	101
50°						110

Tab. 8: GIIC calculated by FEM (J.m^{-2}).

α_1 \ α_2	0°	10°	20°	30°	40°	50°
0°	821	815	890	956	717	a—
10°		821	817	894	960	717
20°			821	818	896	960
30°				821	819	895
40°					823	819
50°						827

[a] Due to the lack of P_C corresponding to $\alpha_{2\text{-}1}$ equal to 50° from tests.

The Mode I fracture equivalent elastic moduli of the lower lamina and upper lamina ($E^*_{I\alpha1}$, $E^*_{II\alpha2}$) could be obtained by using Eq. (2). Likewise, those for Mode II ($E^*_{II\alpha2}$, $E^*_{II\alpha2}$) could be obtained by using Eq. (3), in which E_x is Young's modulus along the longitudinal direction (E_L). As y-axis is in directions ranging from radial (R) to tangential (T) directions, E_y and G_{xy} can be approximated using a Hankinson-type formula (Kretschmann 2010) as follows:

$$E_y = \frac{E_R \times E_T}{E_R \sin^2 \alpha + E_T \cos^2 \alpha} \tag{5}$$

$$G_{xy} = \frac{G_{LR} \times G_{LT}}{G_{LR} \sin^2 \alpha + G_{LT} \cos^2 \alpha} \tag{6}$$

Since μ_{RL} and μ_{TL} are almost of the same value, 0.03 is adopted as μ_{yx}.

By the aid of data fitting techniques, the equivalent elastic modulus of Mode I and II interlaminar fracture (E^*_I, E^*_{II}) can be expressed by Hankinson-type formula as shown in Eqs. (7) and (8), with equivalent elastic modulus of lower lamina ($E^*_{\alpha1}$) and that of upper lamina ($E^*_{\alpha2}$).

$$E^*_I = \frac{0.304 \times E^*_{1\alpha_1} \times E^*_{1\alpha_2}}{E^*_{1\alpha_1} \sin^2 \alpha_{2-1} + E^*_{1\alpha_2} \cos^2 \alpha_{2-1}} \tag{7}$$

$$E^*_{II} = \frac{0.091 \times E^*_{II\alpha_1} \times E^*_{II\alpha_2}}{E^*_{II\alpha_1} \sin^2 \alpha_{2-1} + E^*_{II\alpha_2} \cos^2 \alpha_{2-1}} \tag{8}$$

The fitting results are shown in Fig. 6, where K_{IC} calculated by FEM were compared to those converted from G_{IC} by using Eqs. (7) and (1), likewise for K_{IIC}. The K_{IC} converted from G_{IC} are approximately consistent to those calculated by FEM. Except a few scatter data, the K_{IIC} values converted from G_{IIC} present a good agreement with those calculated by FEM.

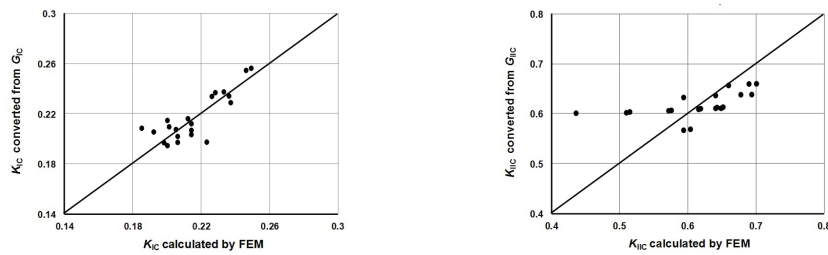

Fig. 6: K_C converted from G_C versus K_C calculated by FEM.

At present, some researchers have addressed the issue of interface fracture toughness of laminate composites, especially fiber-reinforced laminated composites (Andersons and König 2004; Banks-Sills et al. 2005). However, few researches focused on interlaminar facture in glulam (Wang et al. 2012). The authors have conducted DCB and 3ENF tests of glulam in the previous paper (Xu et al. 2016) and the present study attempts to establish a distinct relationship which enables the conversion of G_C to K_C for interlamiar fracture.

CONCLUSIONS

Critical strain energy release rate G_C and stress intensity factors K_C defined as interlaminar fracture toughnesses of glulam can be calculated by FEM. However, there is not a suitable equivalent elastic modulus E^*, which can be used to convert G_C to K_C. This study presented empirical expressions to calculate equivalent elastic moduli for Modes I and II interlaminar fracture of glulam, respectively.

ACKNOWLEDGMENTS

The authors gratefully acknowledge the support of "Key laboratory of basic research projects of Liaoning Province department of education (Grant No. LZ2014010)", "Creative Research Groups of the National Natural Science Foundation of China (Grant No. 51421064)" and "Fundamental Research Funds for the Central Universities (DUT15ZD238)".

REFERENCES

1. Andersons, J., König, M., 2004: Dependence of fracture toughness of composite laminates on interface ply orientations and delamination growth direction. Composites Science and Technology 64(13-14): 2139-2152.
2. ASTM Standard D5528-94a, 2002: Standard test method for mode I interlaminar fracture toughness of unidirectional fiber-reinforced polymer matrix composites.
3. Banks-Sills, L., Boniface, V., Eliasi, R., 2005: Development of a methodology for determination of interface fracture toughness of laminate composites – the 0 /90 pair. International Journal of Solids and Structures 42(2): 663-680.

4. Dassault Systémes Simulia Corp., 2012: 6.12 Abaqus analysis user's manual. Dassault Systémes Simulia Corp. Providence R.I.
5. JIS K7086-1993, 1996: Testing methods for interlaminar fracture toughness of carbon fibre reinforced plastics.
6. Kretschmann, D.E., 2010: Mechanical properties of wood. In: Wood handbook. Pp 26-43, Forest Products Laboratory. Madison.
7. Sih, G.C., Paris, P.C., Irwin, G.R., 1965: On cracks in rectilinearly anisotropic bodies. International Journal of Fracture 1(3): 189-203.
8. Susanti, C.M.E., Nakao, T., Yoshihara, H., 2011: Examination of the mode II fracture behaviour of wood with a short crack in an asymmetric four-point bending test. Engineering Fracture Mechanics 78(16): 2775-2788.
9. Wang, V.Z., Ginger, J.D., Narayan, K., 2012: Intralaminar and interlaminar fracture characterization in glued-laminated timber members using image analysis. Engineering Fracture Mechanics 82: 73-84.
10. Xu, S.L., Reinhardt H.W., Gappoev, M., 1996: Mode II fracture testing method for highly orthotropic materials like wood. International Journal of Fracture 75(3): 185-214.
11. Xu, B.H., Wang, Y.X., Zhao, Y.H., Dong, W., 2016: Influence of growth ring orientation on the interlaminar fracture toughness in glued-laminated timber. Journal of Materials in Civil Engineering, 04016001.

*Bo-Han Xu, Yan-Hua Zhao, Jing-Hua Guo, Ya-Xun Wang
Dalian University of Technology
State Key Laboratory of Coastal and Offshore Engineering
Dalian
China
Phone: +86 0411 84706285
Corresponding author: bohanxu@dlut.edu.cn